Front. Optoelectron. 2020, 13(1): 4–11
https://doi.org/10.1007/s12200-019-0940-3

RESEARCH ARTICLE

Exciton polaritons based on planar dielectric Si asymmetric nanogratings coupled with J-aggregated dyes film

Zhen CHAI[1], Xiaoyong HU (✉)[1,2], Qihuang GONG[1,2]

1 State Key Laboratory for Mesoscopic Physics & Department of Physics, Collaborative Innovation Center of Quantum Matter, Beijing Academy of Quantum Information Sciences, Nano-optoelectronics Frontier Center of Ministry of Education, Peking University, Beijing 100871, China
2 Collaborative Innovation Center of Extreme Optics, Shanxi University, Taiyuan 030006, China

Abstract Optical cavity polaritons, originated from strong coupling between the excitons in materials and photons in the confined cavities field, have recently emerged as their applications in the high-speed low-power polaritons devices, low-threshold lasing and so on. However, the traditional exciton polaritons based on metal plasmonic structures or Fabry-Perot cavities suffer from the disadvantages of large intrinsic losses or hard to integrate and nanofabricate. This greatly limits the applications of exciton poalritons. Thus, here we implement a compact low-loss dielectric photonic – organic nanostructure by placing a 2-nm-thick PVA doped with TDBC film on top of a planar Si asymmetric nanogratings to reveal the exciton polaritons modes. We find a distinct anti-crossing dispersion behavior appears with a 117.16 meV Rabi splitting when varying the period of Si nanogratings. Polaritons dispersion and mode anti-crossing behaviors are also observed when considering the independence of the height of Si, width of Si nanowire B, and distance between the two Si nanowires in one period. This work offers an opportunity to realize low-loss novel polaritons applications.

Keywords exciton polaritons, dielectric Si asymmetric nanogratings, TDBC J-aggregated dyes film

1 Introduction

Confined optical fields [1,2], always appeared in the metallic plasmonic configurations [3–5] and optical cavities [6–8], can possibly produce strong interaction between photons and matters [9] due to the localized photons distributions. When the coupling interaction strengths between cavities photons with resonant excitons are larger than the losses [10], the exciton polaritons can be probably formed. Attributed polaritons condensations and strong nonlinearities inherited from their exciton polaritons, exciton polaritons have exhibited enormous potentials [11] in the field of low-threshold lasers [12–14], all-optical logic devices [15–18] and quantum devices [19–21]. In recent years, many research groups have developed the exciton polaritons nanostructures utilizing the strong coupling between material excitons and confined optical fields in metallic configurations or vertical Fabry Perot cavity and distributed Bragg reflectors (DBRs) [22,23]. The metallic nanostructures [24] are ultracompact but suffer from inherent ohmic losses. Nanostructure DBRs-type exciton polaritons [22,25] are difficult to fabricate and easy to destroy the excitonic material layer. So it is essential to explore novel nanostructures with low losses and flexible structural design and fabrications this field. Last year, Long Zhang et al. [26] have already demonstrated exciton polaritons in silicon nitride half-etching photonic crystals coupled with WSe_2 materials. But due to relative weak optical confinement fields, there are rare exciton polaritons reports directly established on dielectric cavity nanostructures. Therefore, it is still necessary to explore a planar dielectric nanostructure to demonstrate the exciton polaritons.

Here we present a theoretical demonstration of exciton polaritons by strong coupling between photons confined around planar Si asymmetric gratings and excitons in an ultrathin film of J-aggregated dyes. The system consists of periodic asymmetric Si gratings coated by a 2-nm-thick excitonic polymer composite film (poly (vinyl alcohol) (PVA)) doped with J-aggregated molecules (TDBC: 5,6-dichloro-2-[[5,6-dichloro-1-ethyl-3-(4-sulphobutyl)-benzimidazol-2-ylidene]-ropenyl]-1-ethyl-3-(4-sulphobutyl)-benzimidazolium hydroxide, sodium salt, inner salt), so called TDBC-PVA or TDBC for short in this paper) on the

Received May 31, 2019; accepted August 7, 2019

E-mail: xiaoyonghu@pku.edu.cn

SiO_2 substrate. The J-aggregated organic dye molecules exhibit very strong excitonic characteristics, which can exsit stably at the room temperature. Attributed to the localized optical fields between the two Si asymmetric adjacent nanowires and same resonance wavelength, the confined photons in the gap can strongly interact with excitons in the TDBC materials. When the interaction strength is dominant over other losses, the excitons in TDBCs and photons in confined optical field can form the exciton polaritons. This coupling is proved to be an anti-crossing energy dispersion of two polaritons branches. Similar phenomena have been observed in the previous reports [4,27,28] about the metallic plasmonic-exciton nanostructures. The Rabi splitting energy ranges extend about 117.16 meV when coated by a 2-nm-thick TDBC layer. Besides tuning the grating periods, we also discuss the transmission properties in dependence on the height of Si, width of Si nanowire B, and distance between the two Si nanowires in one period. The similar anti-crossing transmission spectra behaviors can further verify the strong interactions between the dielectric nanogratings and TDBC excitonic materials.

2 Sample measurements and discussion

The sample we have explored has been composed of asymmetric dual periodic Si nanogratings with a period of $p = 320$ nm coated by a 2-nm-thick TDBC-PVA film onto fused silica substrates, as shown in Fig. 1(a). The nanowire A and B are shown in Fig. 1(a), respectively. In one period, the nanowire A is the left nanowire with width of w_a, and the nanowire B is the right nanowire with width of w_b. The widths of Si nanowire A and B are 110 and 100 nm, respectively. The distance between the nanowire A and B is only 20 nm to provide an effective confined optical field. The whole dimension of Si gratings is 100 μm×100 μm. The height h of Si nanowire A and B are 100 nm. The TDBC-PVA thin film is chose as 6.0 wt % PVA-water solution with a 2.0 wt % TDBC-water solution in a 1:3 volume ratio, as following the same ratio in Ref. [29]. Due to the negative real part of permittivity about TDBC-PVA, the metallic-like optical dielectric characteristics of TDBC-PVA film are displayed in Fig. 1(b), where they correspond to the exciton wavelength 590 nm. We use a dielectric Si nanograting to match the resonance of TDBC excitons at the room temperature. The resonant wavelength of pure Si asymmetric nanogratings without TDBC is 568 nm with a transmission ratio 0.014 using software *Comsol Multiphysics* (shown in Fig. 1(c)), whose full width at half maximum extends 45 nm. And from the electric field distributions at the resonance wavelength (Fig. 1(d)), we can observe the optical field distributed in the narrow gap between the Si nanowire A and B with a maximum intensity of 8.4 a.u. and extended to the upper air surrounding. The confinement optical field is the basic to obtain Rabi splitting dispersion spectra of exciton polaritons in this system with different interaction strengths between Si nanogratings photons and TDBC excitons. The optical transmission spectrum of Si nanogratings-TDBC excited by the x-polarized light at the perpendicular illumination is displayed in Fig. 1(e). The two separated resonance dips around the exciton wavelength 590 nm of TDBC appeared at the wavelength 568 nm with a transmission ratio of 0.038 and 598 nm with 0.11, which correspond to high-energy and low-energy polariton modes, respectively. Because of the wavelength mismatch between the Si nanograting resonance and TDBC absorption, the splitting transmission spectrum is not symmetrical. The transmission ratio at exciton wavelength 590 nm have a maximum value 0.16.

To study the dielectric Si asymmetric gratings-TDBC exciton coupling system, the period of Si gratings is varied, which directly induces to a resonant wavelength mode shift of Si nanogratings, coming from the variation of the interaction strength between the TDBC and Si nanogratings. The period-dependent optical transmission spectra of Si nanogratings-TDBC system and Si nanogratings perpendicularly illuminated by the x-polarized light are shown in Figs. 2(a) and 2(b), respectively. When the period changes from 290 to 400 nm, there are always being for the Rabi splitting phenomenon. For the maximum period 400 nm, one transmission dip corresponding to the upper polariton branch (UPB) is located at the wavelength 585 nm, which increases with the decreasing of period. Another transmission dip corresponding to the lower polariton branch (LPB) appears at the wavelength 630 nm. Along with the reduction of the period, the UPB and LPB undergo an anti-crossing transmission decreasing (as the white dotted line shown in Fig. 2(a)). The anti-crossing center wavelength is the exciton wavelength (black dotted line) of TDBC film. The transmission spectrum shows an almost symmetric line shape on the condtion of the period 340 nm, which indicates that the Rabi splitting energy at this period is almost 117.16 meV. At the crossing period point, the polaritons are half-photon and half-exciton quasi-particles. Similarly, we also consider the transmission properties of the Si nanogratings without the TDBC films from the period 290 to 400 nm. Only a transmission dip appears at the wavelength 546 nm when the period of Si nanogratings is 290 nm, while 623 nm when the period is 400 nm. The tunable resonance mode shift of the dielectric Si nanogratings allow us to explore the coupling strength as a function of nanogratings period in the hybrid system. To confirm strong coupling, we use the transmission minimum values of the hybrid system with different Si nanograting periods to fit the coupling strength (Fig. 2(c)). Because there are a large number of excitons in TDBC involved in our photon-exciton coupling system, the coupled harmonic oscillator model is enough to provide physical images, which is also a standard and common model in the field of exciton polaritons [26].

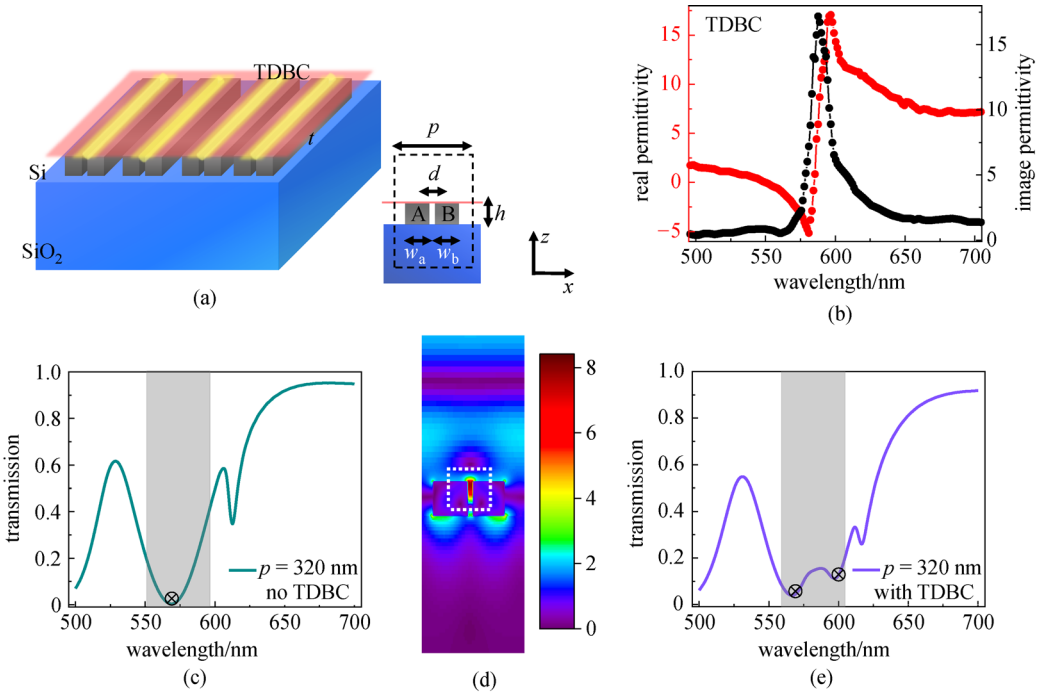

Fig. 1 Characteristics of planar dielectric Si asymmetric nanogratings and TDBC film. (a) Schematic illustration of planar dielectric Si asymmetric nanogratings-TDBC film system. The width of Si nanowire A and B are w_a= 110 nm and w_b= 100 nm, respectively. The distance of narrow gap between the Si nanowire A and B is d = 20 nm. The period of Si nanogratings is p = 320 nm. The yellow regions stand for confined optical fields of this system. (b) Real and image permittivity parts of PVA doped with TDBC film. (c) Transmission spectrum of a 320-nm-wide periodic Si nanogratings without TDBC film under the x-polarized incident beam. (d) Electric field distributions of Si nanogratings at the resonance wavelength 568 nm. (e) Transmission spectrum of the Si nanogratings-TDBC coupled system

The energies of polariton modes can be viewed as [26]

$$E_{\mathrm{UP,LP}} = \frac{1}{2}\left(E_{\mathrm{photon}} + E_{\mathrm{exciton}} + \mathrm{i}(\gamma_{\mathrm{photon}} + \gamma_{\mathrm{exciton}})/2\right) \pm \sqrt{g^2 + \frac{1}{4}[E_{\mathrm{photon}} - E_{\mathrm{exciton}} + \mathrm{i}(\gamma_{\mathrm{photon}} - \gamma_{\mathrm{exciton}})]^2}, \quad (1)$$

where $E_{\mathrm{UP,LP}}$ are the energies of upper and lower photon-exciton coupling mode branches, respectively. E_{photon} and E_{exciton} are the energies of the uncoupled Si nanogratings resonance photons and TDBC, and g is the exciton-photon coupling strength. γ_{photon} and $\gamma_{\mathrm{exciton}}$ correspond to the dispersion rates, which are full linewidth at half maximum of the Si nanogratings cavity mode and TDBC excitonic absorption spectra, respectively. When $\gamma_{\mathrm{exciton}}$ and $\gamma_{\mathrm{exciton}}$ are smaller than their energies, the image part of polariton modes can been neglected.

Under this condition, the polariton modes can be seen as

$$E_{\mathrm{UP,LP}} = \frac{1}{2}(E_{\mathrm{photon}} + E_{\mathrm{exciton}}) \pm \sqrt{g^2 + \frac{1}{4}[E_{\mathrm{photon}} - E_{\mathrm{exciton}}]^2}. \quad (2)$$

A Rabi splitting $2\hbar\,\Omega = 2\sqrt{g^2 - \frac{1}{4}(\gamma_{\mathrm{photon}} - \gamma_{\mathrm{exciton}})^2}$ requires this system to match the condition $g > \frac{|\gamma_{\mathrm{photon}} - \gamma_{\mathrm{exciton}}|}{2}$ when considering the strong coupling. Besides, the Rabi spilitting must exceed the sum of the half linewidths of the photonic mode and excitonic mode for an actually observable strong coupling. From the pure Si nanogratings photonic transmission resonant spectrum and the refractive index dispersion curve of TDBC material (corresponding to its absorption), we can clearly find γ_{photon} = 152 meV, E_{exciton} = 2.1 eV, $\gamma_{\mathrm{exciton}}$ = 54 meV. By fitting the transmission minima in Fig. 2(b) to the coupled oscillator model, we can extract the coupling strength g = 58.58 meV (here, E_{photon} is determined by the

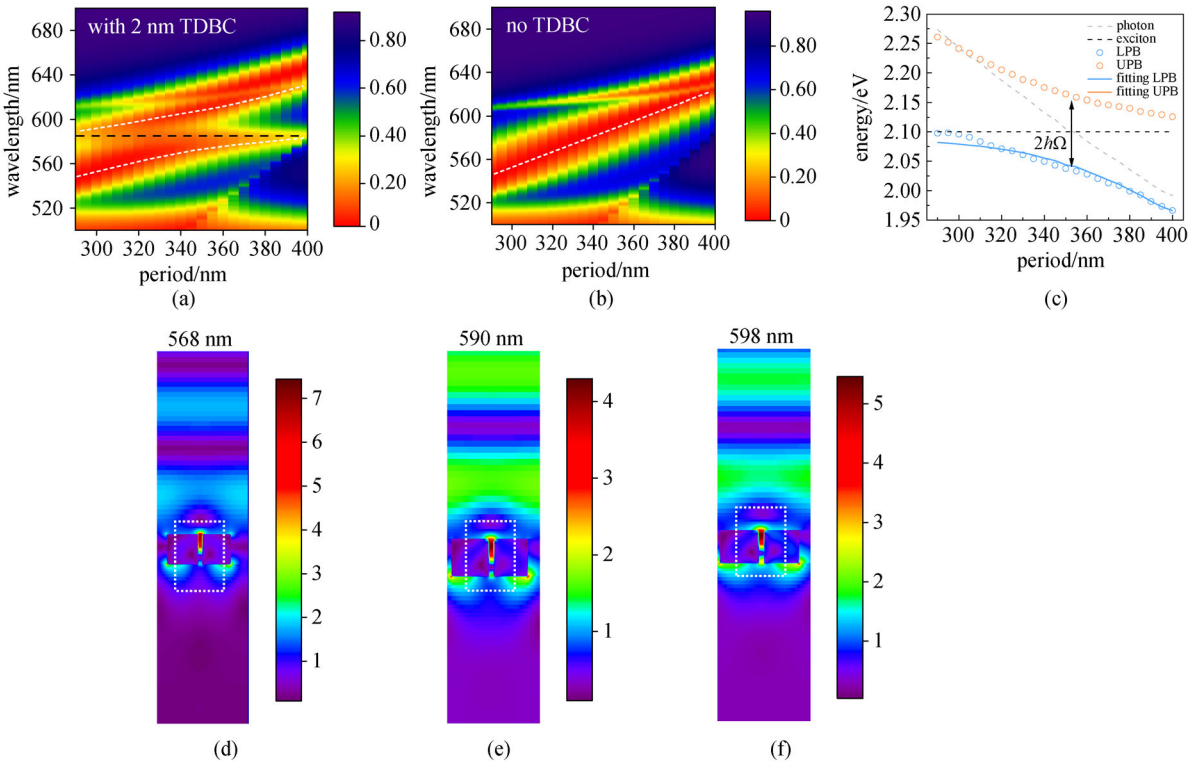

Fig. 2 Calculated transmission characteristics of dielectric Si asymmetric gratings-TDBC exciton system in dependence on the period of Si gratings under the *x*-polarized incident beam. (a) and (b) are transmission spectra of dielectric Si asymmetric gratings with TDBC film and without TDBC film by tuning the period from 290 to 400 nm. (c) Energy of the UPB (orange bubbles) and LPB (bule bubbles) as a function of Si nograings periods. The solid lines are fit by the coupled oscillator model. The dashed lines are the energies of uncoupled Si nanogratings resonance minima and TDBC excitons. The double-headed arrow stands for the Rabi splitting energy. (d), (e) and (f) are the electric field distributions of Si gratings-TDBC film system when the period of Si nanogratings is 320 nm at the UPB wavelength 568 nm, exciton wavelength 590 nm, LPB wavelength 598 nm

transmission ratio minima from Fig. 2(a)), corresponding to a Rabi splitting energies of $2\hbar\,\Omega \sim 2g|_{\delta=0} = 117.16$ meV (the detuning $\delta = E_{\text{photon}} - E_{\text{exciton}}$), which is in agreement with the dispersion spectra. Therefore, the interaction satisfies the coupling strength $g > \left(\frac{|\gamma_{\text{photon}} - \gamma_{\text{exciton}}|}{2} = 52.2 \text{ meV}\right)$, which identifies our hybrid system well meet the criterion of the strong coupling. However, we can find that it does not strictly satisfy the observation condition of two spectral peaks for the Rabi splitting energy (Rabi splitting $2\hbar\,\Omega >$ polariton full width half maximum $\gamma_{\text{photon}} + \gamma_{\text{exciton}}$, but it is close [30]. So this conclusion is in accordance with a not-big-enough transmission value at the detuning-zero wavelength. Figures 2(d)–2(f) show the normalized electric field distributions of dielectric Si nanogratings-TDBC system with a period of 320 nm at the wavelength 568, 590 and 598 nm, which corresponds to the UPB, exciton wavelength and LPB, respectively. We can observe that all the optical fields are almost confined in the narrow gaps between the Si nanowire A and B for these three wavelengths, but have different electric field intensities and color bars. For the condition of Si nanograting period 320 nm, the UPB is largely photon-like and shares more optical field intensities, while the LPB is exciton-like and becomes more photon-like with the increasing of periods. Meanwhile, the electric field intensity of the two polariton branches are relatively weaker than that in the Si nanogratings without the TDBC film, depicted in Fig. 1 (d). Obviously, this is due to the fact that the exciton components of polaritons stand for absorption in the simulations, which can weaken the optical field intensities at the polaritons branches. These results confirm the formation of exciton polaritons associated with large Rabi splitting in the dielectric Si nanogratings-TDBC system.

To further confirm strong coupling, we study independently the calculated transmission spectra of dielectric Si nanogratings-TDBC film system in dependence on the height of Si, width of Si nanowire B, and the narrow distance between Si nanowire A and B. The standard reference sizes for the system are the same as we used before, $w_a = 110$ nm, $w_b = 100$ nm, $h = 100$ nm, $d = 20$ nm, $p = 320$ nm and $t = 2$ nm, respectively. Figure 3(a) corresponds to a series of transmission spectra of the Si nanogratings-TDBC film system under the condition of

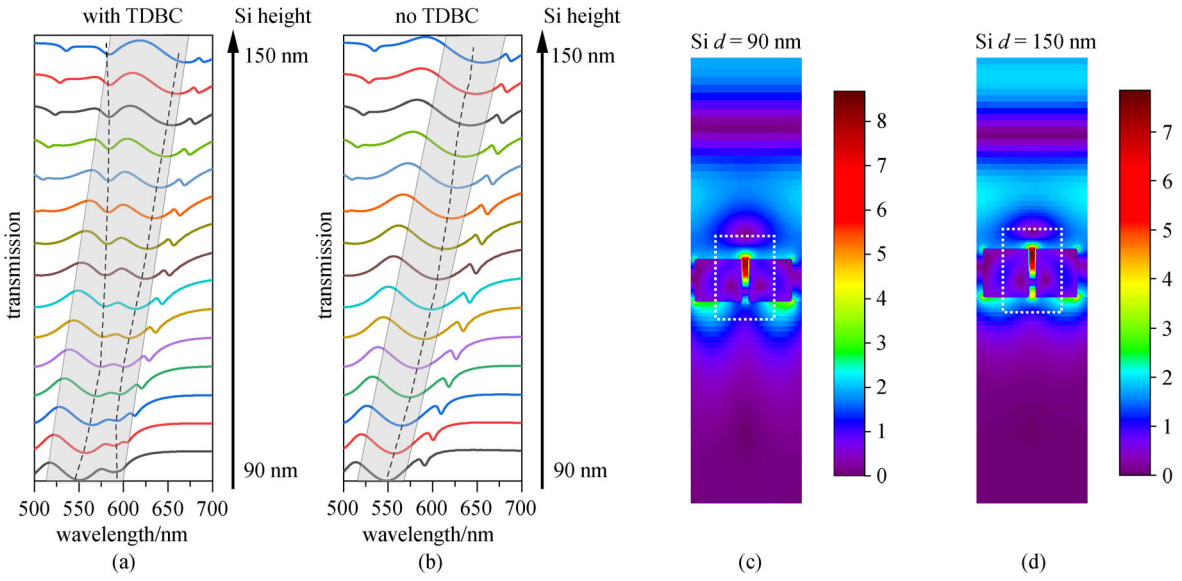

Fig. 3 Transmission properties of Si asymmetric nanogratings coupled with TDBC and without TDBC in dependence on the height of Si nanowires from 90 to 150 nm. (a) and (b) are the corresponding transmission spectra, respectively. And (c) and (d) are the Si nanogratings without TDBC film at the height of Si nanogratings $d = 90$ nm and $d = 150$ nm, respectively

different heights of Si nanowires. It has been shown that the center of anti-crossing transmission spectra appears when the Si nanowires height is h = 106 nm, where the corresponding Rabi splitting wavelength range is about 30 nm. For 90-nm-high Si nanowires, the splitting we obtain is well observed at the wavelength 546 nm with line widths of 31 nm (full width at half maximum, FWHM) and 591 nm with line widths of 19 nm as the upper (UPB) and lower (LPB) polariton branch, respectively. Similarly, the UPB shows a larger proportion of photon components in dielectric nanogratings, while the LPB tends to excitons. When the height of Si nanowires grows to 150 nm, the splitting phenomenon shows a similar avoided crossing with 581 nm (line widths of 21 nm) as UPB and 665 nm (line widths of 34 nm) as LPB, respectively. In this condition, the UPB shares more excitonic components, and the LPB behaves opposite. In contrast, without the TDBC layer, an individual and sharp resonant mode is calculated by software *Comsol Multiphysics* for Si nanogratings through tuning the height of dielectric Si nanowires from 90 to 150 nm (Fig. 3(b)). The resonant photonic modes linearly shift from the wavelength 548 nm (with line widths of 36 nm) to 649 nm (with line widths of 48 nm), located between the UPB and LPB in coupled system. Figures 3(c) and 3(d) show the calculated electric field distributions of the dielectric Si nanogratings photonic mode with $d = 90$ nm and $d = 150$ nm, respectively. For both Si nanowire heights, we observe the optical field confined in the narrow gaps between Si nanowire A and B at the resonant dip wavelength. The confined field intensity shows stronger in the Si nanowire $d = 90$ nm than that in the condition of $d = 150$ nm. Thus, this phenomenon is in agreement with the excitonic or photonic component ratios of two polariton branches in our coupled system.

Similar strong interactions can be obtained with Si nanowires of different widths and distances. In Fig. 4, we summarize the simulated results obtained by *Comsol Multiphysics*. We calculate the transmission properties of the coupling polaritons modes (Fig. 4(a)) and the uncoupling dielectric grating photonic modes (Fig. 4(b)) via changing the widths of Si nanowire B. The transmission spectra maintain basically minor changes with the increase of Si nanowire B widths. For 80-nm-wide Si nanowire B, the coupled splitting line shape is asymmetric, in which the strength of UPB is more larger than that of the LPB. The UPB is located at the wavelength 552 nm with line widths of 20 nm and transmission ratio of 0.06, while the LPB is located at the wavelength 579 nm with line widths of 20 nm and transmission ratio of 0.22. When the width of Si nanowire B is 140 nm, the condition behaves opposite. The UPB wavelength is 572 nm with line widths of 21 nm, and the LPB is 603 nm with a 10-nm-wide transmission dip. Moreover, it is important to note that, in our system, the different widths of Si nanowire B make smaller influence on the uncoupling photonic modes in the dielectric Si nanogratings compared with the Si nanowire height. The resonant wavelength of the pure Si nanogratings photonic mode turns red-shift from 554 to 579 nm with almost the same line widths when the width of Si nanowire B increases from 80 to 140 nm, which further demonstrates that the confined optical field of Si nanogratings comes from x component of the electric field. Besides, we also study that the dielectric Si nanogratings photons-TDBC excitons interactions can be

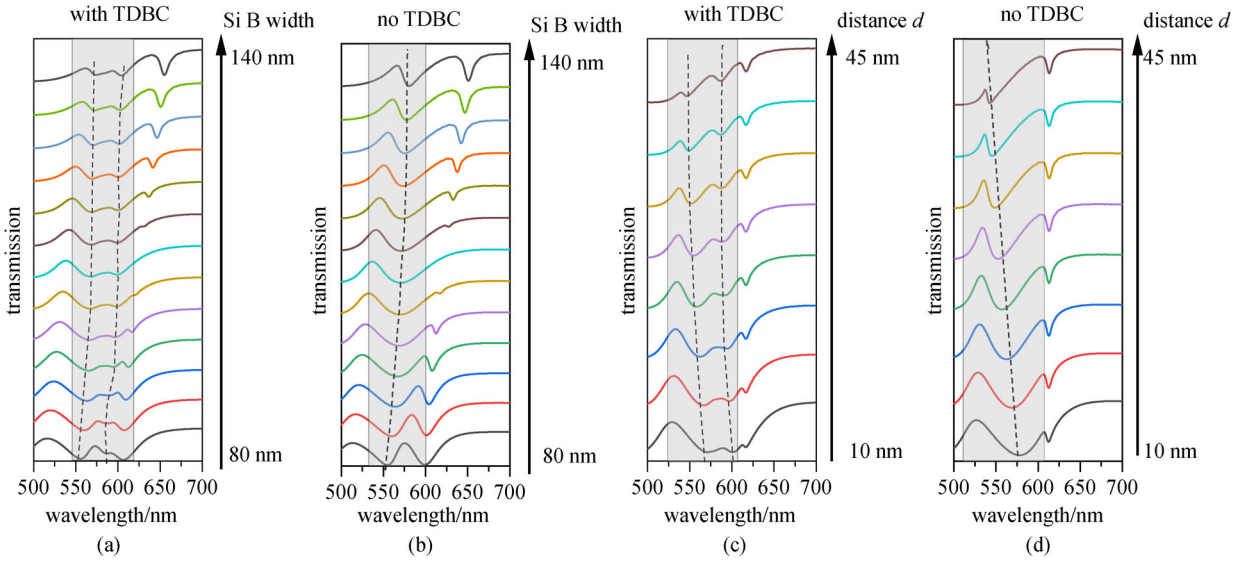

Fig. 4 Transmission spectra of Si nanogratings interacted with TDBC film or without TDBC film in dependence on the width of Si nanowire B from 80 to 140 nm ((a) and (b)) and distance of the narrow gap between the Si nanowire A and B from 10 to 45 nm ((c) and (d)), respectively

efficiently tuned by controlling the distance of the narrow gap between Si nanowire A and B in one period (Figs. 4(c) and 4(d)). In particular, as the distance increases, the whole transmission spectra of the hybrid system become blue-shift, induced by the blue-shift of dielectric Si nanogratings photonic mode. The two polaritons branch wavelengths of the dielectric photons-TDBC excitons hybrid system are 570 and 600 nm, respectively, when the distance is 10 nm. While the two branches are 547 and 588 nm with a 60-nm-wide distance. The corresponding dielectric photonic resonant mode is 576 and 544 nm, respectively.

3 Conclusion

In summary, we realize an exciton polaritons system based on the planar dielectric Si asymmetric nanogratings interacted with a 2-nm-thick PVA doped with TDBC J-aggregate dye film on the SiO_2 substrate. The narrow gaps between dielectric Si asymmetric nanowires provide a relative confined optical field distribution. The exciton polaritons in this system are originated from the confined photons in the Si nanogratings and excitons in the PVA-TDBC J-aggregated dye film. We observe a series of anti-crossing transmission spectra with a 117.16 meV-energy range Rabi splitting when scanning the period of Si nanogratings from 290 to 400 nm. The splitting independences of the height of Si, width of Si nanowire B, and distance between the two Si nanowires in one period about this dielectric Si-TDBC film are also studied. More generally, our findings open up a possibility to exploit the exciton polaritons in the dielectric photonic nanostructures coupled with excitonic materials. Comparing with the metallic plasmonic-exciton system (typical dispersion rate value, $\gamma_{plasmon} \sim > 200$ meV), the form of dielectric photon-exciton interaction systems possesses less inherent losses ($\gamma_{photon} \sim 152$ meV), which will effectively increase the transmission contrast ratios and propagation lengths, thus expanding the potential application fields of exciton polaritons. Future exploration can be focused on the novel photonic nanostructure using low-loss dielectric materials instead of Si in the visible wavelength range and temporal dynamic process studies of dielectric photon-exciton interaction system, and practical configurations in all-polaritons devices and circuits based on the dielectric photon-exciton polaritons system.

Acknowledgements This work was supported by the National Key Research and Development Program of China (Grant No. 2018YFB2200403), the National Natural Science Foundation of China (Grant Nos. 61775003, 11734001, 11527901, and 11804008), the National Postdoctoral Program for Innovative Talents (No. BX201700011), and the China Postdoctoral Science Foundation (No. 2018M630019), and Beijing Municipal Science & Technology Commission (No. Z191100007219001).

Competing financial interests The authors declare that they have no competing financial interests.

References

1. Liu X, Menon V M. Control of light-matter interaction in 2D atomic crystals using microcavities. IEEE Journal of Quantum Electronics, 2015, 51(10): 1–8

2. Törmä P, Barnes W L. Strong coupling between surface plasmon polaritons and emitters: a review. Reports on progress in physics. Physical Society (Great Britain), 2015, 78(1): 013901
3. Ren J, Gu Y, Zhao D, Zhang F, Zhang T, Gong Q. Evanescent-vacuum-enhanced photon-exciton coupling and fluorescence collection. Physical Review Letters, 2017, 118(7): 073604
4. Wang S, Li S, Chervy T, Shalabney A, Azzini S, Orgiu E, Hutchison J A, Genet C, Samorì P, Ebbesen T W. Coherent coupling of WS2 monolayers with metallic photonic nanostructures at room temperature. Nano Letters, 2016, 16(7): 4368–4374
5. Lin Q Y, Li Z, Brown K A, O'Brien M N, Ross M B, Zhou Y, Butun S, Chen P C, Schatz G C, Dravid V P, Aydin K, Mirkin C A. Strong coupling between plasmonic gap modes and photonic lattice modes in DNA-assembled gold nanocube arrays. Nano Letters, 2015, 15(7): 4699–4703
6. Guo X, Zou C L, Jung H, Tang H X. On-chip strong coupling and efficient frequency conversion between telecom and visible optical modes. Physical Review Letters, 2016, 117(12): 123902
7. van Vugt L K, Rühle S, Ravindran P, Gerritsen H C, Kuipers L, Vanmaekelbergh D. Exciton polaritons confined in a ZnO nanowire cavity. Physical Review Letters, 2006, 97(14): 147401
8. Sun Y, Yoon Y, Steger M, Liu G, Pfeiffer L N, West K, Snoke D W, Nelson K A. Direct measurement of polariton–polariton interaction strength. Nature Physics, 2017, 13(9): 870–875
9. Baranov D G, Wersäll M, Cuadra J, Antosiewicz T J, Shegai T. Novel nanostructures and materials for strong light–matter interactions. ACS Photonics, 2018, 5(1): 24–42
10. Vasa P, Wang W, Pomraenke R, Lammers M, Maiuri M, Manzoni C, Cerullo G, Lienau C. Real-time observation of ultrafast Rabi oscillations between excitons and plasmons in metal nanostructures with J-aggregates. Nature Photonics, 2013, 7(2): 128–132
11. Sanvitto D, Kéna-Cohen S. The road towards polaritonic devices. Nature Materials, 2016, 15(10): 1061–1073
12. Byrnes T, Kim N Y, Yamamoto Y. Exciton–polariton condensates. Nature Physics, 2014, 10(11): 803–813
13. Schneider C, Rahimi-Iman A, Kim N Y, Fischer J, Savenko I G, Amthor M, Lermer M, Wolf A, Worschech L, Kulakovskii V D, Shelykh I A, Kamp M, Reitzenstein S, Forchel A, Yamamoto Y, Höfling S. An electrically pumped polariton laser. Nature, 2013, 497 (7449): 348–352
14. Paschos G G, Somaschi N, Tsintzos S I, Coles D, Bricks J L, Hatzopoulos Z, Lidzey D G, Lagoudakis P G, Savvidis P G. Hybrid organic-inorganic polariton laser. Scientific Reports, 2017, 7(1): 11377
15. Amo A, Liew T C H, Adrados C, Houdre R, Giacobino E, Kavokin A V, Bramati A. Exciton-polariton spin switches. Nature Photonics, 2010, 4(6): 361–366
16. De Giorgi M, Ballarini D, Cancellieri E, Marchetti F M, Szymanska M H, Tejedor C, Cingolani R, Giacobino E, Bramati A, Gigli G, Sanvitto D. Control and ultrafast dynamics of a two-fluid polariton switch. Physical Review Letters, 2012, 109(26): 266407
17. Fraser M D. Coherent exciton-polariton devices. Semiconductor Science and Technology, 2017, 32(9): 093003
18. Solnyshkov D D, Bleu O, Malpuech G. All optical controlled-NOT gate based on an exciton–polariton circuit. Superlattices and Microstructures, 2015, 83: 466–475
19. Bose R, Sridharan D, Kim H, Solomon G S, Waks E. Low-photon-number optical switching with a single quantum dot coupled to a photonic crystal cavity. Physical Review Letters, 2012, 108(22): 227402
20. Demirchyan S S, Chestnov I Y, Alodjants A P, Glazov M M, Kavokin A V. Qubits based on polariton Rabi oscillators. Physical Review Letters, 2014, 112(19): 196403
21. Solnyshkov D D, Johne R, Shelykh I A, Malpuech G. Chaotic Josephson oscillations of exciton-polaritons and their applications. Physical Review B, 2009, 80(23): 235303
22. Gao T, Eldridge P S, Liew T C H, Tsintzos S I, Stavrinidis G, Deligeorgis G, Hatzopoulos Z, Savvidis P G. Polariton condensate transistor switch. Physical Review B, 2012, 85(23): 235102
23. Antón C, Liew T C H, Sarkar D, Martín M D, Hatzopoulos Z, Eldridge P S, Savvidis P G, Viña L. Operation speed of polariton condensate switches gated by excitons. Physical Review B, 2014, 89(23): 235312
24. Gonçalves P A D, Bertelsen L P, Xiao S S, Mortensen N A. Plasmon-exciton polaritons in two-dimensional semiconductor/metal interfaces. Physical Review B, 2018, 97(4): 041402 (R)
25. Su R, Diederichs C, Wang J, Liew T C H, Zhao J, Liu S, Xu W, Chen Z, Xiong Q. Room-temperature polariton lasing in all-inorganic perovskite nanoplatelets. Nano Letters, 2017, 17(6): 3982–3988
26. Zhang L, Gogna R, Burg W, Tutuc E, Deng H. Photonic-crystal exciton-polaritons in monolayer semiconductors. Nature Communications, 2018, 9(1): 713
27. Wang H, Toma A, Wang H Y, Bozzola A, Miele E, Haddadpour A, Veronis G, De Angelis F, Wang L, Chen Q D, Xu H L, Sun H B, Zaccaria R P. The role of Rabi splitting tuning in the dynamics of strongly coupled J-aggregates and surface plasmon polaritons in nanohole arrays. Nanoscale, 2016, 8(27): 13445–13453
28. Fofang N T, Grady N K, Fan Z, Govorov A O, Halas N J. Plexciton dynamics: exciton-plasmon coupling in a J-aggregate-Au nanoshell complex provides a mechanism for nonlinearity. Nano Letters, 2011, 11(4): 1556–1560
29. Gentile M J, Núñez-Sánchez S, Barnes W L. Optical field-enhancement and subwavelength field-confinement using excitonic nanostructures. Nano Letters, 2014, 14(5): 2339–2344
30. Zheng D, Zhang S, Deng Q, Kang M, Nordlander P, Xu H. Manipulating coherent plasmon-exciton interaction in a single silver nanorod on monolayer WSe_2. Nano Letters, 2017, 17(6): 3809–3814

Zhen Chai is a postdoctor of Prof. Qihuang Gong at Peking University. Now she majors in the study of the design of two-dimensional materials-nanostructures exciton polaritons and its application in optical devices.

Xiaoyong Hu is a Cheung Kong professor of physics at Peking University. Prof. Hu's current research interests include photonic crystals, plasmonics, topological photonics and integrated photonic devices.

Qihuang Gong is a member of the Chinese Academy Sciences and Vice President at Peking University, China, where he is also the founding director of the Institute of Modern Optics. Prof. Gong's current research interests are ultrafast optics, nonlinear optics, mesoscopic quantum optics and optical devices for applications.